Eur. Phys. J. C 44, 147–159 (2005)
Digital Object Identifier (DOI) 10.1140/epjc/s2005-02353-3

THE EUROPEAN PHYSICAL JOURNAL C

Flavour independent searches for hadronically decaying neutral Higgs bosons

The DELPHI Collaboration

J. Abdallah[25], P. Abreu[22], W. Adam[51], P. Adzic[11], T. Albrecht[17], T. Alderweireld[2], R. Alemany-Fernandez[8], T. Allmendinger[17], P. Allport[23], U. Amaldi[29], N. Amapane[45], S. Amato[48], E. Anashkin[36], A. Andreazza[28], S. Andringa[22], N. Anjos[22], P. Antilogus[25], W-D. Apel[17], Y. Arnoud[14], S. Ask[26], B. Asman[44], E. Augustin[25], A. Augustinus[8], P. Baillon[8], A. Ballestrero[46], P. Bambade[20], R. Barbier[27], D. Bardin[16], J. Barker[17], A. Baroncelli[39], M. Battaglia[8], M. Baubillier[25], K-H. Becks[53], M. Begalli[6], A. Behrmann[53], E. Ben-Haim[20], N. Benekos[32], A. Benvenuti[5], C. Berat[14], M. Berggren[25], L. Bernтzon[44], D. Bertrand[2], M. Besancon[40], N. Besson[40], D. Bloch[9], M. Blom[31], M. Bluj[52], M. Bonesini[29], M. Boonekamp[40], L. Booth[23], G. Borisov[21], O. Botner[49], B. Bouquet[20], V. Bowcock[23], I. Boyko[16], M. Bracko[43], R. Brenner[49], E. Brodet[35], P. Bruckman[18], M. Brunet[7], L. Bugge[33], P. Buschmann[53], M. Calvi[29], T. Camporesi[8], V. Canale[38], F. Carena[8], N. Castro[22], F. Cavallo[5], M. Chapkin[42], Ph. Charpentier[8], P. Checchia[36], R. Chierici[8], P. Chliapnikov[42], J. Chudoba[8], U. Chung[8], K. Cieslik[18], P. Collins[8], R. Contri[13], G. Cosme[20], F. Cossutti[47], J. Costa[50], D. Crennell[37], J. Cuevas[34], J. D'Hondt[2], J. Dalmau[44], T. da Silva[48], W. Da Silva[25], G. Della Ricca[47], A. De Angelis[47], W. De Boer[17], C. De Clercq[2], B. De Lotto[47], N. De Maria[45], A. De Min[36], L. de Paula[48], L. Di Ciaccio[38], A. Di Simone[39], K. Doroba[52], J. Drees[53,8], M. Dris[32], G. Eigen[4], T. Ekelof[49], M. Ellert[49], M. Elsing[8], C. Espirito Santo[22], G. Fanourakis[11], D. Fassouliotis[11,3], M. Feindt[17], J. Fernandez[41], A. Ferrer[50], F. Ferro[13], U. Flagmeyer[53], H. Foeth[8], E. Fokitis[32], F. Fulda-Quenzer[20], J. Fuster[50], M. Gandelman[48], C. Garcia[50], Ph. Gavillet[8], E. Gazis[32], R. Gokieli[8,52], B. Golob[43], G. Gomez-Ceballos[41], P. Goncalves[22], E. Graziani[39], G. Grosdidier[20], K. Grzelak[52], J. Guy[37], C. Haag[17], A. Hallgren[49], K. Hamacher[53], K. Hamilton[35], S. Haug[33], F. Hauler[17], V. Hedberg[26], M. Hennecke[17], H. Herr[8], J. Hoffman[52], S-O. Holmgren[44], J. Holt[8], A. Houlden[23], K. Hultqvist[44], N. Jackson[23], G. Jarlskog[26], P. Jarry[40], D. Jeans[35], K. Johansson[44], D. Johansson[44], P. Jonsson[27], C. Joram[8], L. Jungermann[17], F. Kapusta[25], S. Katsanevas[27], E. Katsoufis[32], G. Kernel[43], P. Kersevan[8,43], U. Kerzel[17], A. Kiiskinen[15], T. King[23], J. Kjaer[8], P. Kluit[31], P. Kokkinias[11], C. Kourkoumelis[3], O. Kouznetsov[16], Z. Krumstein[16], M. Kucharczyk[18], J. Lamsa[1], G. Leder[51], F. Ledroit[14], L. Leinonen[44], R. Leitner[30], J. Lemonne[2], V. Lepeltier[20], T. Lesiak[18], W. Liebig[53], D. Liko[51], A. Lipniacka[44], H. Lopes[48], M. Lopez[34], D. Loukas[11], P. Lutz[40], L. Lyons[35], J. MacNaughton[51], A. Malek[53], S. Maltezos[32], F. Mandl[51], J. Marco[41], R. Marco[41], B. Marechal[48], M. Margoni[36], J-C. Marin[8], C. Mariotti[8], A. Markou[11], C. Martinez-Rivero[41], J. Masik[12], N. Mastroyiannopoulos[11], F. Matorras[41], C. Matteuzzi[29], F. Mazzucato[36], M. Mazzucato[36], R. Mc Nulty[23], C. Meroni[28], E. Migliore[45], W. Mitaroff[51], U. Mjoernmark[26], T. Moa[44], M. Moch[17], K. Moenig[8,10], R. Monge[13], J. Montenegro[31], D. Moraes[48], S. Moreno[22], P. Morettini[13], U. Mueller[53], K. Muenich[53], M. Mulders[31], L. Mundim[6], W. Murray[37], B. Muryn[19], G. Myatt[35], T. Myklebust[33], M. Nassiakou[11], F. Navarria[5], K. Nawrocki[52], R. Nicolaidou[40], M. Nikolenko[16,9], A. Oblakowska-Mucha[19], V. Obraztsov[42], A. Olshevski[16], A. Onofre[22], R. Orava[15], K. Osterberg[15], A. Ouraou[40], A. Oyanguren[50], M. Paganoni[29], S. Paiano[5], P. Palacios[23], H. Palka[18], D. Papadopoulou[32], L. Pape[8], C. Parkes[24], F. Parodi[13], U. Parzefall[8], A. Passeri[39], O. Passon[53], L. Peralta[22], V. Perepelitsa[50], A. Perrotta[5], A. Petrolini[13], J. Piedra[41], L. Pieri[39], F. Pierre[40], M. Pimenta[22], E. Piotto[8], T. Podobnik[43], V. Poireau[8], E. Pol[6], G. Polok[18], V. Pozdniakov[16], N. Pukhaeva[2,16], A. Pullia[29], J. Rames[12], A. Read[33], P. Rebecchi[8], J. Rehn[17], D. Reid[31], R. Reinhardt[53], P. Renton[35], F. Richard[20], J. Ridky[12], M. Rivero[41], D. Rodriguez[41], A. Romero[45], P. Ronchese[36], P. Roudeau[20], T. Rovelli[5], V. Ruhlmann-Kleider[40], D. Ryabtchikov[42], A. Sadovsky[16], L. Salmi[15], J. Salt[50], C. Sander[17], A. Savoy-Navarro[25], U. Schwickerath[8], A. Segar[35], R. Sekulin[37], M. Siebel[53], A. Sisakian[16], G. Smadja[27], O. Smirnova[26], A. Sokolov[42], A. Sopczak[21], R. Sosnowski[52], T. Spassov[8], M. Stanitzki[17], A. Stocchi[20], J. Strauss[51], B. Stugu[4], M. Szczekowski[52], M. Szeptycka[52], T. Szumlak[19], T. Tabarelli[29], C. Taffard[23], F. Tegenfeldt[49], J. Timmermans[31], L. Tkatchev[16], M. Tobin[23], S. Todorovova[12], B. Tome[22], A. Tonazzo[29], P. Tortosa[50], P. Travnicek[12], D. Treille[8], G. Tristram[7], M. Trochimczuk[52], C. Troncon[28], M-L. Turluer[40], A. Tyapkin[16], P. Tyapkin[16], S. Tzamarias[11], V. Uvarov[42], G. Valenti[5], P. Van Dam[31], J. Van Eldik[8], A. Van Lysebetten[2], N. van Remortel[2], I. Van Vulpen[8], G. Vegni[28], F. Veloso[22], W. Venus[37], P. Verdier[27], V. Verzi[38], D. Vilanova[40], L. Vitale[47], V. Vrba[12], H. Wahlen[53], J. Washbrook[23], C. Weiser[17], D. Wicke[8], J. Wickens[2], G. Wilkinson[35], M. Winter[9], M. Witek[18], O. Yushchenko[42], A. Zalewska[18], P. Zalewski[52], D. Zavrtanik[43], V. Zhuravlov[16], I. Zimin[16], A. Zintchenko[16], M. Zupan[11]

[1] Department of Physics and Astronomy, Iowa State University, Ames IA 50011-3160, USA
[2] Physics Department, Universiteit Antwerpen, Universiteitsplein 1, 2610 Antwerpen, Belgium
and IIHE, ULB-VUB, Pleinlaan 2, 1050 Brussels, Belgium
and Faculté des Sciences, Univ. de l'Etat Mons, Av. Maistriau 19, 7000 Mons, Belgium
[3] Physics Laboratory, University of Athens, Solonos Str. 104, 10680 Athens, Greece
[4] Department of Physics, University of Bergen, Allégaten 55, 5007 Bergen, Norway
[5] Dipartimento di Fisica, Università di Bologna and INFN, Via Irnerio 46, 40126 Bologna, Italy
[6] Centro Brasileiro de Pesquisas Físicas, rua Xavier Sigaud 150, 22290 Rio de Janeiro, Brazil
and Depto. de Física, Pont. Univ. Católica, C.P. 38071 22453 Rio de Janeiro, Brazil
and Inst. de Física, Univ. Estadual do Rio de Janeiro, rua São Francisco Xavier 524, Rio de Janeiro, Brazil
[7] Collège de France, Lab. de Physique Corpusculaire, IN2P3-CNRS, 75231 Paris Cedex 05, France
[8] CERN, 1211 Geneva 23, Switzerland
[9] Institut de Recherches Subatomiques, IN2P3 - CNRS/ULP - BP20, 67037 Strasbourg Cedex, France
[10] Now at DESY-Zeuthen, Platanenallee 6, 15735 Zeuthen, Germany
[11] Institute of Nuclear Physics, N.C.S.R. Demokritos, P.O. Box 60228, 15310 Athens, Greece
[12] FZU, Inst. of Phys. of the C.A.S. High Energy Physics Division, Na Slovance 2, 180 40, Praha 8, Czech Republic
[13] Dipartimento di Fisica, Università di Genova and INFN, Via Dodecaneso 33, 16146 Genova, Italy
[14] Institut des Sciences Nucléaires, IN2P3-CNRS, Université de Grenoble 1, 38026 Grenoble Cedex, France
[15] Helsinki Institute of Physics, P.O. Box 64, 00014 University of Helsinki, Finland
[16] Joint Institute for Nuclear Research, Dubna, Head Post Office, P.O. Box 79, 101 000 Moscow, Russian Federation
[17] Institut für Experimentelle Kernphysik, Universität Karlsruhe, Postfach 6980, 76128 Karlsruhe, Germany
[18] Institute of Nuclear Physics PAN,Ul. Radzikowskiego 152, 31142 Krakow, Poland
[19] Faculty of Physics and Nuclear Techniques, University of Mining and Metallurgy, 30055 Krakow, Poland
[20] Université de Paris-Sud, Lab. de l'Accélérateur Linéaire, IN2P3-CNRS, Bât. 200, 91405 Orsay Cedex, France
[21] School of Physics and Chemistry, University of Lancaster, Lancaster LA1 4YB, UK
[22] LIP, IST, FCUL - Av. Elias Garcia, 14-1°, 1000 Lisboa Codex, Portugal
[23] Department of Physics, University of Liverpool, P.O. Box 147, Liverpool L69 3BX, UK
[24] Dept. of Physics and Astronomy, Kelvin Building, University of Glasgow, Glasgow G12 8QQ
[25] LPNHE, IN2P3-CNRS, Univ. Paris VI et VII, Tour 33 (RdC), 4 place Jussieu, 75252 Paris Cedex 05, France
[26] Department of Physics, University of Lund, Sölvegatan 14, 223 63 Lund, Sweden
[27] Université Claude Bernard de Lyon, IPNL, IN2P3-CNRS, 69622 Villeurbanne Cedex, France
[28] Dipartimento di Fisica, Università di Milano and INFN-MILANO, Via Celoria 16, 20133 Milan, Italy
[29] Dipartimento di Fisica, Univ. di Milano-Bicocca and INFN-MILANO, Piazza della Scienza 2, 20126 Milan, Italy
[30] IPNP of MFF, Charles Univ., Areal MFF, V Holesovickach 2, 180 00, Praha 8, Czech Republic
[31] NIKHEF, Postbus 41882, 1009 DB Amsterdam, The Netherlands
[32] National Technical University, Physics Department, Zografou Campus, 15773 Athens, Greece
[33] Physics Department, University of Oslo, Blindern, 0316 Oslo, Norway
[34] Dpto. Fisica, Univ. Oviedo, Avda. Calvo Sotelo s/n, 33007 Oviedo, Spain
[35] Department of Physics, University of Oxford, Keble Road, Oxford OX1 3RH, UK
[36] Dipartimento di Fisica, Università di Padova and INFN, Via Marzolo 8, 35131 Padua, Italy
[37] Rutherford Appleton Laboratory, Chilton, Didcot OX11 OQX, UK
[38] Dipartimento di Fisica, Università di Roma II and INFN, Tor Vergata, 00173 Rome, Italy
[39] Dipartimento di Fisica, Università di Roma III and INFN, Via della Vasca Navale 84, 00146 Rome, Italy
[40] DAPNIA/Service de Physique des Particules, CEA-Saclay, 91191 Gif-sur-Yvette Cedex, France
[41] Instituto de Fisica de Cantabria (CSIC-UC), Avda. los Castros s/n, 39006 Santander, Spain
[42] Inst. for High Energy Physics, Serpukov P.O. Box 35, Protvino, (Moscow Region), Russian Federation
[43] J. Stefan Institute, Jamova 39, 1000 Ljubljana, Slovenia
and Laboratory for Astroparticle Physics, Nova Gorica Polytechnic, Kostanjeviska 16a, 5000 Nova Gorica, Slovenia
and Department of Physics, University of Ljubljana, 1000 Ljubljana, Slovenia
[44] Fysikum, Stockholm University, Box 6730, 113 85 Stockholm, Sweden
[45] Dipartimento di Fisica Sperimentale, Università di Torino and INFN, Via P. Giuria 1, 10125 Turin, Italy
[46] INFN, Sezione di Torino, and Dipartimento di Fisica Teorica, Università di Torino, Via P. Giuria 1, 10125 Turin, Italy
[47] Dipartimento di Fisica, Università di Trieste and INFN, Via A. Valerio 2, 34127 Trieste, Italy
and Istituto di Fisica, Università di Udine, 33100 Udine, Italy
[48] Univ. Federal do Rio de Janeiro, C.P. 68528 Cidade Univ., Ilha do Fundão 21945-970 Rio de Janeiro, Brazil
[49] Department of Radiation Sciences, University of Uppsala, P.O. Box 535, 751 21 Uppsala, Sweden
[50] IFIC, Valencia-CSIC, and D.F.A.M.N., U. de Valencia, Avda. Dr. Moliner 50, 46100 Burjassot (Valencia), Spain
[51] Institut für Hochenergiephysik, Österr. Akad. d. Wissensch., Nikolsdorfergasse 18, 1050 Vienna, Austria
[52] Inst. Nuclear Studies and University of Warsaw, Ul. Hoza 69, 00681 Warsaw, Poland
[53] Fachbereich Physik, University of Wuppertal, Postfach 100 127, 42097 Wuppertal, Germany

Received: 11 January 2005 / Revised version: 24 June 2005 /
Published online: 20 September 2005 –

Abstract. This paper describes flavour independent searches for hadronically decaying neutral Higgs bosons in the data collected by the DELPHI experiment at LEP, at centre-of-mass energies between 189 and 209 GeV. The collected data-set corresponds to an integrated luminosity of around 610 pb^{-1}. The $\mathrm{e^+e^-} \to \mathrm{hA}$ and $\mathrm{e^+e^-} \to \mathrm{hZ}$ processes are considered, with direct Higgs boson decays into hadrons. No evidence for Higgs boson production is found, and cross-section limits are set as a function of the Higgs boson masses. No explicit assumptions are made on the underlying physics beyond the Standard Model, allowing interpretation of the data in a large class of models.

1 Introduction

As long as bosonic decay channels are kinematically closed, the Standard Model (SM) Higgs boson decays preferentially into the heaviest accessible fermion pair. This leads to the dominance of Higgs boson decays to b quarks in most of the mass range accessible at LEP. In extensions of the SM, however, the Higgs boson couplings to b quarks might well be suppressed. This can for example occur in the Minimal Supersymmetric Standard Model (MSSM) [1], and in general Two Higgs Doublet Models (2HDM) [2]. Suppressed couplings to b-quarks are also possible in models with composite Higgs and gauge bosons, where the dominant Higgs boson decay channel is gluonic [3]. The SM Higgs boson search at LEP strongly relies on the identification of b quarks or τ leptons to separate a possible signal from background processes, and has reduced sensitivity to the final states predicted by such alternative models.

This paper presents searches that only assume direct hadronic decays of the Higgs bosons. The scope of these analyses is thus more general, and encompasses the models referred to above. However, rather than stating the results in explicit theoretical frameworks, model independent bounds on production cross-sections are derived, allowing to confront a wide class of models with the data.

Two Higgs boson production processes are studied in this paper: the Higgsstrahlung process $\mathrm{e^+e^-} \to \mathrm{hZ}$, and Higgs boson pair production $\mathrm{e^+e^-} \to \mathrm{hA}$, which is present in all extensions of the Standard Model Higgs sector beyond one doublet. Although the notation is familiar from CP conserving models, the CP properties of h and A are not necessarily specified here.

Flavour independent searches for hadronic Higgs boson decays have been published by the other LEP collaborations [4–6].

The paper is organized as follows. The common framework and search strategy is described in Sect. 2, and is followed by an overview of the experimental setup and the data sets in Sect. 3. The search for hadronic decays of hA pairs is described in Sect. 4. Section 5 describes the search for hZ production, where the Higgs boson is accompanied by jets, missing energy, electrons, or muons from the Z boson decay. Section 6 combines the various analyses, and gives flavour independent results on the hZ and hA cross-sections, as a function of the Higgs boson masses. Section 7 concludes the paper.

2 General features

The analyses presented in this paper rely essentially on kinematic and event shape information. Without the background rejection allowed by b quark or τ lepton identification, the signal contamination by quark pair production and/or vector boson pair production can be important, and dijet mass information must be used to discriminate signal from background. The way in which this information is exploited depends on the search channel, and is detailed in the corresponding sections.

The search results independence from the hadronic flavour of the Higgs bosons decay products is obtained by considering only the decay mode with lowest sensitivity in each search channel. The precise procedure varies again from one channel to the other, and details are given for each analysis in the corresponding description.

All search results presented in this work are interpreted using a modified frequentist technique based on the extended likelihood ratio [7]. For a given experiment, the test statistic Q is defined as the likelihood ratio of the signal+background hypothesis (s+b) to the background hypothesis (b), computed from the number of observed and expected events in both hypotheses. Measured discriminating variables can be used to assign a signal to background ratio to individual events. Probability density functions (PDFs) for Q in the b and s+b hypotheses are built using Monte Carlo sampling of the expected background and signal rates, and of the optional discriminating variable distributions. The confidence levels $\mathrm{CL_b}$ and $\mathrm{CL_{s+b}}$ are defined as the integrals of the b and s+b PDFs for Q between $-\infty$ and the observed value Q_{obs}.

A signal hypothesis to which there is no sensitivity might be uncorrectly excluded by $\mathrm{CL_{s+b}}$ in case a downward fluctuation of the data occurs. To prevent this, we adopt the conservative approach of defining the confidence level in the signal hypothesis, $\mathrm{CL_s}$, as the ratio $\mathrm{CL_{s+b}}/\mathrm{CL_b}$. 1-$\mathrm{CL_s}$ measures the confidence with which the signal hypothesis can be rejected, and will be larger than 0.95 for an exclusion confidence of 95%.

When no signal is found, upper bounds on the production cross-section times the branching fraction into hadrons are extracted for both production processes as a function of the Higgs boson masses. These bounds are expressed in terms of reference cross-sections, defined as follows. The production rate of any final state resulting from $\mathrm{e^+e^-} \to \mathrm{hZ}$ can be expressed in terms of the SM hZ cross-section, $\sigma_{\mathrm{hZ}}^{\mathrm{SM}}$ [8]. The reference cross-section for $\mathrm{e^+e^-} \to \mathrm{hA}$, $\sigma_{\mathrm{hA}}^{\mathrm{ref}}$, is calculated with `HZHA` [9], assuming the 2HDM and the absence of any mixing in the Higgs sector. The result depends only on electroweak parameters and the h and A Higgs boson masses, and remains valid for models with any number of Higgs doublets or singlets. Suppression terms coming from branching fractions and possible suppression of the Higgs boson couplings to the Z

(such factors are hereafter denoted by BR and R, respectively) all factorize, and are hidden in a generic (model independent) suppression factor:

$$\begin{aligned}\sigma_{\mathrm{hZ}\to\mathrm{Z+hadrons}} &= \sigma^{\mathrm{SM}}_{\mathrm{hZ}} \times R_{\mathrm{hZ}} \times BR(\mathrm{h}\to\mathrm{hadrons}) \\ &\equiv \sigma^{\mathrm{SM}}_{\mathrm{hZ}} \times C^2_{\mathrm{hZ}}; \\ \sigma_{\mathrm{hA}\to\mathrm{hadrons}} &= \sigma^{\mathrm{ref}}_{\mathrm{hA}} \times R_{\mathrm{hA}} \times BR(\mathrm{h}\to\mathrm{hadrons}) \\ &\quad \times BR(\mathrm{A}\to\mathrm{hadrons}) \\ &\equiv \sigma^{\mathrm{ref}}_{\mathrm{hA}} \times C^2_{\mathrm{hA}}\end{aligned}$$

Our results will be expressed in terms of C^2_{hZ} and C^2_{hA}.

Although the traditional CP-conserving Higgs boson nomenclature is used throughout the paper, part of the results can also be extended to the context of CP-violating Higgs sectors. For hA production, the parity and charge conjugation properties of the Higgs bosons do not play any role in the decay kinematics. The results on C^2_{hA} are therefore universally valid for the pair production of any two Higgs bosons (i.e. $\mathrm{h_i h_j} \to$ hadrons), regardless of their CP properties. On the contrary, our results on $\mathrm{e^+e^-} \to \mathrm{hZ}$ assume standard quantum numbers for the Higgs boson. Non-standard Higgs boson parity properties would imply different polarization of the associated Z boson, thereby affecting the angular distributions of the bosons and the selection efficiencies. Our results for this channel should therefore be used with care.

If kinematically open and allowed by the Higgs boson quantum numbers, cascade decays like $\mathrm{h}\to\mathrm{AA}$ may become dominant. The efficiency of the analyses developed below to these final states has not been evaluated.

The study also applies to non-Higgs scalar particles. The cross-sections and analyses presented here however assume that the produced scalars have negligible width (less than about $1\,\mathrm{GeV/c^2}$).

3 Detector, data samples and simulation

A detailed description of the DELPHI detector and its performance during the LEP1 data taking period can be found in [10]. For LEP2, the vertex detector was upgraded [11], and scintillator counters were added in regions without electromagnetic calorimetry (at 40 and 90 degrees from the beam axis), improving the detection of events with radiative photons in these regions. The detector was operated in nominal conditions until September 2000, when one of the twelve sectors of DELPHI's main tracking device underwent an irremediable failure. A special algorithm, based on complementary subdetectors, allowed to limit the tracking efficiency loss in this region.

The data samples used in this paper were collected during the last 3 years of LEP operation (1998 to 2000), and are clustered around seven centre-of-mass energy values, as shown in Table 1. The total used luminosity amounts to $610.4\,\mathrm{pb^{-1}}$. The hZ analysis uses the data from all listed sets, while the hA search uses all but the two sets with lowest luminosity.

Table 1. Centre-of-mass energy and integrated luminosity of the data collected by the DELPHI detector in the years 1998–2000

year	1998		1999			2000	
$\sqrt{s}$ (GeV)	188.6	191.6	195.5	199.5	201.6	205.0	206.5
$\mathcal{L}$ ($\mathrm{pb^{-1}}$)	158.0	25.9	76.9	84.3	41.1	82.0	142.2

The simulation samples used for this study have been produced at the centre-of-mass energies given in Table 1; details are given below. In all cases, samples have been processed that comply with the experimental situation before and after the detector failure mentioned above.

For the hZ channel, two-fermion background events are simulated using the `KK2F` [12] generator, while `WPHACT` [13] is used for four-fermion final states (see [14] for the specific DELPHI implementation). For the hA analysis, prepared during an earlier stage of this work, the two-fermion and four-fermion SM backgrounds are simulated using the `PYTHIA` [15] and `EXCALIBUR` [16] generators respectively. Backgrounds from two-photon events are generated using `PYTHIA`. All background samples have a size equivalent to 20–50 times the luminosity recorded at the corresponding centre-of-mass energy.

The `HZHA` generator is used to generate hZ signal samples for $40 \le m_{\mathrm{h}} \le 120\,\mathrm{GeV/c^2}$, in steps of $2.5\,\mathrm{GeV/c^2}$. Z boson decays into quarks, neutrinos, electrons and muons are simulated, and the Higgs boson is decaying to either a pair of gluons, or a pair of light quarks (s quarks in practice); at several mass points, samples with Higgs boson decays into heavy quarks are used to verify the flavour-independence of the results. For the neutrino channel, signal samples are also generated every $5\,\mathrm{GeV/c^2}$ for $10 \le m_{\mathrm{h}} \le 40\,\mathrm{GeV/c^2}$, and at $m_{\mathrm{h}} = 4\,\mathrm{GeV/c^2}$; heavy quark samples are simulated at all mass points (when kinematically allowed) in this case. All hZ signal samples contain 5000 events.

The hA process is also simulated using the `HZHA` generator, in the mass range $16 \le m_{\mathrm{h}} + m_{\mathrm{A}} \le 180\,\mathrm{GeV/c^2}$. The simulation starts at $m_{\mathrm{h}}, m_{\mathrm{A}} = 4\,\mathrm{GeV/c^2}$; steps of $5\,\mathrm{GeV/c^2}$ are used when $10 \le m_{\mathrm{h}}, m_{\mathrm{A}} \le 30\,\mathrm{GeV/c^2}$; $10\,\mathrm{GeV/c^2}$ steps are used otherwise. Higgs boson decays into gluon or light quark pairs are simulated over the whole mass range; samples with heavy quarks are simulated at several mass points for cross-checks. All hA signal samples contain 2000 events.

For low Higgs boson masses, the decay final state is determined by non-perturbative mechanisms (direct coupling to hadronic resonances). There is no robust model of this regime, and the efficiencies of the analyses described below are difficult to predict. We therefore limit our search to Higgs boson masses above $4\,\mathrm{GeV/c^2}$, where the `PYTHIA` hadronization model is expected to be valid.

4 Search for hA production

The flavour-independent hA search is designed to cover a large part of the accessible h and A mass range, and is

based on general kinematic features such as event shapes and dijet mass information.

The higher multiplicity of gluon jets compared to quark jets results in a higher selection efficiency for hA $\rightarrow$ gluons, but also in a worse mass resolution for this signal. To minimize biases that may arise from these competing effects, the selection efficiencies are determined using samples of hA $\rightarrow$ quarks, while the mass reconstruction is done with samples of hA $\rightarrow$ gluons.

4.1 Analysis streams

A first preselection is applied to all events, requiring at least 20 charged particles, a total reconstructed energy greater than 60% of the centre-of-mass energy, and an effective centre-of-mass energy after initial state radiation greater than 150 GeV (the method used to estimate the effective centre-of-mass energy is described in [17]). The efficiencies of the multiplicity cut are typically 98% for the hA $\rightarrow$ quarks signal samples, and 100% for the hA $\rightarrow$ gluons samples.

In the rest of the analysis, three different sets of cuts are designed to obtain sufficient signal acceptance over a large domain in the (m_{h},m_{A})-plane. The analysis streams are described below.

4.1.1 Four-jet stream

Close to the kinematic limit and when both Higgs bosons have comparable masses, a four-jet topology is expected. To analyse this topology, events are clustered into four jets with the DURHAM algorithm [18]. All jets are required to have an invariant mass larger than $2\,\mathrm{GeV/c^2}$, and to contain at least two charged particles. Events are retained in this stream if their thrust value is below 0.85 and if the product of the smallest jet energy and inter-jet angle (called $\mathrm{E_{min}}\alpha_{\mathrm{min}}$) is greater than $10\,\mathrm{GeV}\cdot\mathrm{rad}$. Dijet invariant mass information is used to reject events compatible with WW production as in [19], requiring the corresponding probability, $\mathrm{P_{WW}}$, to be less than 0.01. This proves helpful not only when $m_{\mathrm{h}} = m_{\mathrm{A}} \sim 80\,\mathrm{GeV/c^2}$, but also for other signal masses, where WW production contributes to the expected background through wrong jet pairings.

4.1.2 Three-jet stream

When the h and A mass difference increases, the events tend to contain three jets, since the jets resulting from the decay of the lighter Higgs boson cannot always be resolved. The same behaviour is observed if h and A both have low masses, because of the larger boost in this case. To analyse this topology, only events with thrust values between 0.70 and 0.92 are kept. Events are then clustered into four jets, and events compatible with WW production are rejected as in the four-jet stream. The remaining events are clustered into three jets. As before, all jets are required to have a mass larger than $2\,\mathrm{GeV/c^2}$ and to contain at least two charged particles.

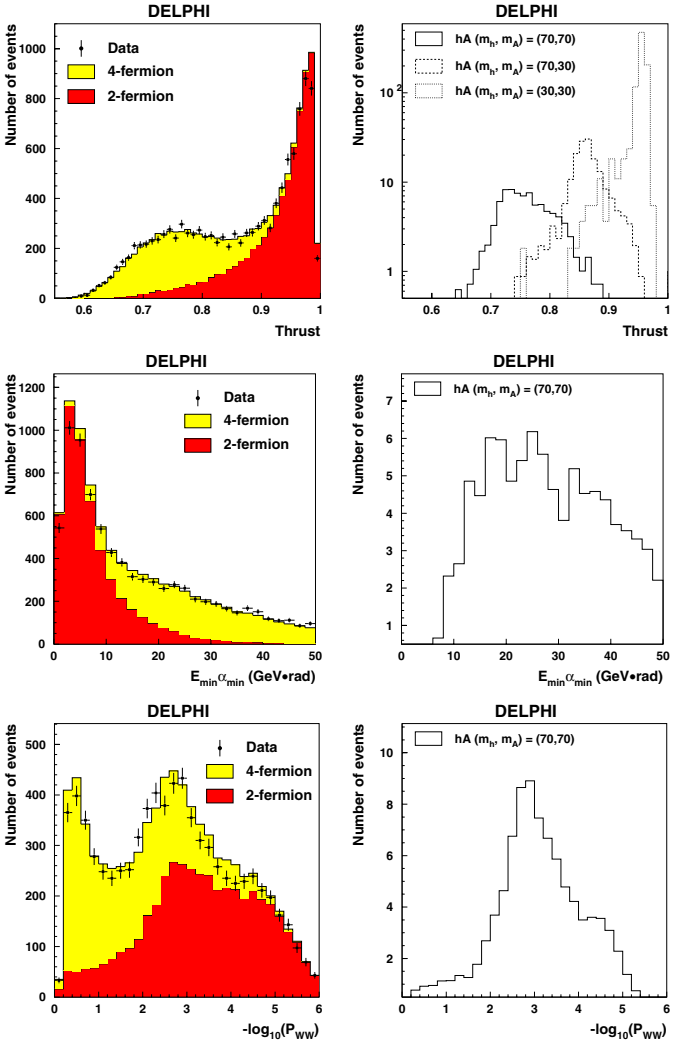

Fig. 1. hA search. Comparison between data and simulation for the variables used in the three selection streams, at the preselection level. Thrust, $\mathrm{E_{min}}\alpha_{\mathrm{min}}$, and -$\log_{10}(\mathrm{P_{WW}})$ are shown from top to bottom. The signal normalization assumes $C^2_{\mathrm{hA}} = 1$. The discriminating power is indicated by corresponding distributions from representative signal samples. In particular, the thrust distributions justify the use of three complementary selection streams

4.1.3 High-thrust stream

Finally, when both Higgs bosons are sufficiently light, signal events tend to become cigar-like. Events are selected in this analysis stream if they have a thrust value larger than 0.92, and are clustered into three jets, each jet having to satisfy the same quality criteria as above. As the dominant background comes from two-quark processes, the kinematic compatibility with W-pair events is not tested.

4.1.4 Comparison between data and simulation

Distributions of thrust, $\mathrm{E_{min}}\alpha_{min}$ and $-\log_{10}\mathrm{P_{WW}}$ are shown in Fig. 1 for example signals representative of the three analysis streams. Their performance and complementarity are illustrated in Table 2. As discussed above, these

efficiencies are obtained assuming h and A decays into light quark pairs. From comparisons with a number of samples with Higgs boson decays into b quarks, the quark flavour-dependence of the efficiencies is found smaller than 2%. The efficiencies obtained with gluonic Higgs boson decays are higher by a factor up to 1.2 in the three-jet and four-jet analyses, and by a factor up to 2 in the high-thrust analysis. A numerical comparison between data and expected background is shown in Table 3.

4.2 Final discriminant variable

In all three analysis streams, a four-constraint fit is performed on the selected events, requiring total energy and momentum conservation. The compatibility of each event with a given mass hypothesis $(m_{\mathrm{h}}, m_{\mathrm{A}})$ is estimated using the following quantity :

$$\chi^2(m_{\mathrm{h}}, m_{\mathrm{A}}) = \left(\frac{m_1^{\mathrm{rec}} - m_{\mathrm{h}}}{\delta m_1^{\mathrm{rec}}}\right)^2 + \left(\frac{m_2^{\mathrm{rec}} - m_{\mathrm{A}}}{\delta m_2^{\mathrm{rec}}}\right)^2 .$$

In the above expression, m_1^{rec} is the mass of a given dijet, m_2^{rec} is the mass of the opposite dijet in the four-jet stream, and of the opposite jet in the other streams, and $\delta m_{1,2}^{\mathrm{rec}}$ are the corresponding errors as obtained from the kinematic fit. For every event, the jet pairing that minimizes $\chi^2(m_{\mathrm{h}}, m_{\mathrm{A}})$ is used to compute the discriminant.

The distributions of this variable are computed, for data and background, on a $1\,\mathrm{GeV/c^2} \times 1\,\mathrm{GeV/c^2}$ grid in the $(m_{\mathrm{h}}, m_{\mathrm{A}})$-plane.

Table 2. hA search. Efficiencies of the three analysis streams on three classes of hA signal events, considered as four-jet events when m_{h},$m_{\mathrm{A}} > 60\,\mathrm{GeV/c^2}$; as high-thrust events when m_{h},$m_{\mathrm{A}} < 30\,\mathrm{GeV/c^2}$; and as three-jet events in the remaining cases

Signal	$\epsilon_{\mathrm{hA}}^{\mathrm{four-jet}}(\%)$	$\epsilon_{\mathrm{hA}}^{\mathrm{three-jet}}(\%)$	$\epsilon_{\mathrm{hA}}^{\mathrm{high-thrust}}(\%)$
Four-jet events	~ 70	~ 45	0–5
Three-jet events	~ 50	~ 70	0–5
High-thrust events	0–5	0–5	10–15

Table 3. hA search. Numerical comparison between data and background simulation, after all selections. The year 2000 data are merged in the last column. The statistical uncertainty on the background estimates is 2%

centre-of-mass energy	189 GeV	196 GeV	200 GeV	>204.5 GeV
Four-jet stream :				
expected background	433.5	221.3	259.0	634.5
observed events	459	248	232	642
Three-jet stream :				
expected background	1593.3	750.6	797.0	1894.3
observed events	1585	736	772	1824
High-thrust stream :				
expected background	1384.9	642.5	654.3	1516.3
observed events	1331	612	607	1450

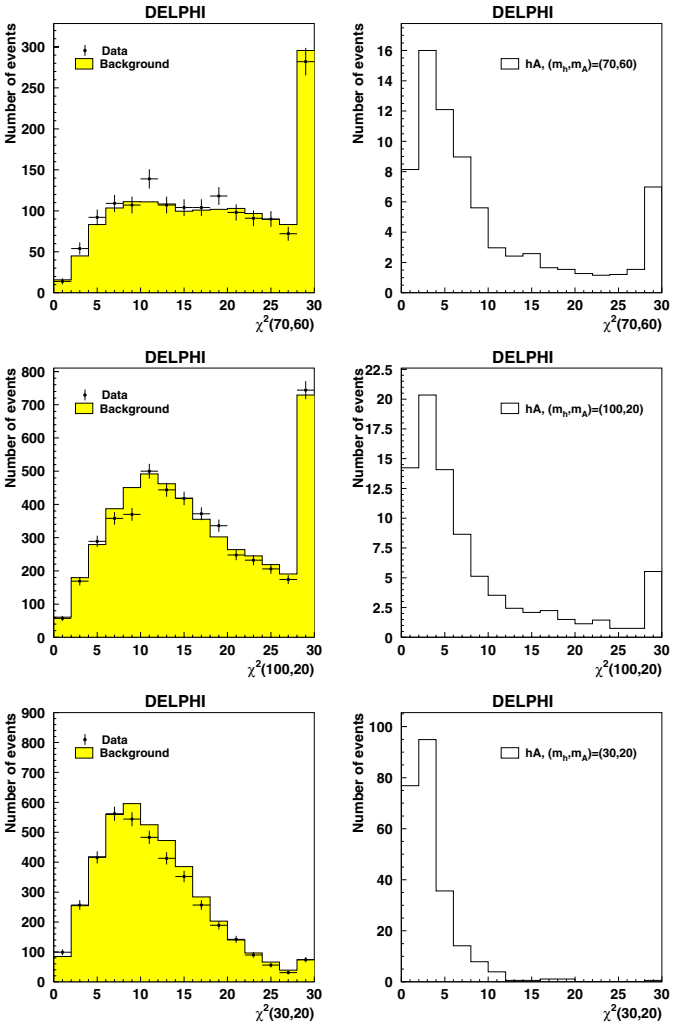

Fig. 2. hA search. Comparison between data and simulation for the distributions of $\chi^2(m_{\mathrm{h}}, m_{\mathrm{A}})$. The discrimination obtained for $(m_{\mathrm{h}},m_{\mathrm{A}}) = (70,60)$ in the four-jet stream, for $(m_{\mathrm{h}},m_{\mathrm{A}}) = (100,20)$ in the three-jet stream, and for $(m_{\mathrm{h}},m_{\mathrm{A}}) = (30,20)$ in the high-thrust stream are shown from top to bottom. In all distributions, overflows have been included in the last bin. All the data used for this search are included (cf. Sect. 3). The signal normalization assumes $C_{\mathrm{hA}}^2 = 1$

The signal distributions are first determined at the simulated mass points. To construct the signal distributions at mass configurations that are not simulated, the histograms are linearly interpolated between the three closest simulated points. The validity of this procedure is discussed in the next section.

These distributions are used for the statistical evaluation of the compatibility of the data with the simulation following the procedure described in Sect. 2. Figure 2 illustrates this procedure for three representative example signals.

4.3 Systematic uncertainties

Systematic uncertainties affecting this analysis are related to imperfect simulation of the detector and of SM processes,

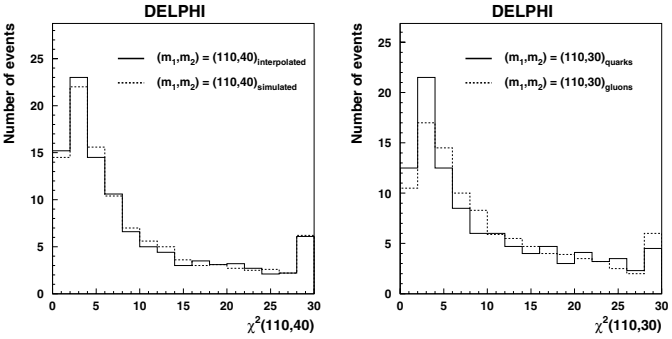

Fig. 3. hA search. Left: distribution of $\chi^2(110,40)$, as obtained from an interpolation between the nearest simulated samples at (m_h,m_A)=(110,30) and (110,50) GeV/c^2. It is compared with the true (dashed line) distribution from a simulated sample at (m_h,m_A)=(110,40). Right: distribution of $\chi^2(110,30)$ for Higgs bosons decaying into either $q\bar{q}$ (solid line) or gg (dashed line), reflecting the worse mass resolution obtained for a four-gluon final state. In all distributions, overflows have been included in the last bin

to residual flavour-dependence of the selections, and to the signal interpolation procedure. All effects are discussed below.

The numerical differences at the preselection level between the observed data and the expectation from SM processes are taken as a first contribution to the uncertainty on the background prediction. For every subsequent selection variable, the difference of the average values of the corresponding distributions in data and background is computed; the selection cut is then varied by this amount. This procedure leads to an estimated systematic uncertainty on the backgrounds of 5% in the four-jet and three-jet streams, and 10% in the high-thrust stream, at each centre-of-mass energy. The higher uncertainty in the high-thrust stream is mainly due to the observed numerical discrepancy after the preselection.

As stated earlier, the flavour-dependence of the selection efficiencies is estimated by comparing the results obtained for gluon decays, light quark decays, and b-quark decays. The preselection efficiency is slightly worse (by at most 2%) in the case of light quark decays, and is applied to the gluon decays as well. The remaining selections have a quark flavour dependence smaller than 2%. This number is taken as a contribution to the systematic uncertainty on the signal rate.

Possible uncertainties from the interpolation procedure are illustrated in Fig. 3, which compares a simulated distribution with the result of an interpolation between neighbouring points. The shapes are well reproduced. To quantify more precisely what accuracy can be expected from this procedure, the previous exercise is repeated on a large number of simulated mass configurations. In each case, the bin contents of the simulated and interpolated histograms are compared. The distribution of the ratio of true and interpolated bin contents has a spread of 5%, which is taken as a second contribution to the systematic uncertainty on the signal rate. Note that this is a conservative estimate as the real interpolation is over smaller intervals than the 20 GeV/c^2 used here.

Figure 3 also shows the discriminant variable distribution obtained for quarks and gluons, at (m_h,m_A)=(110,30). As expected, the worse mass resolution on gluon jets translates into a somewhat reduced discriminating power; this is true for all mass points. The present analysis, using a selection efficiency determined on light-quark signal samples and a kinematic analysis calibrated on gluon samples, thus has no bias towards a given flavour that would invalidate the results when considering other Higgs boson hadronic decays.

5 Search for hZ production

This section describes a flavour-independent search for the $e^+e^- \to hZ$ process. The analyses used in this section are adapted from those used for the DELPHI $e^+e^- \to ZZ$ and $e^+e^- \to Z\gamma^*$ cross-section measurements [19, 20], or from the previous section. The analyses are briefly described in the following; we refer to the original publications for further details.

5.1 Final states with jets

The hZ search in the fully hadronic final state is described below. Two mass regions are analysed separately, namely $m_h < 40$ GeV/c^2 using a three-jet analysis, and $m_h > 40$ GeV/c^2 using a four-jet analysis.

5.1.1 Low mass search ($m_h < 40$ GeV/c^2)

The region $4 < m_h < 40$ GeV/c^2 is analysed using the hA three-jet stream, described in Sect. 4.1. Efficiencies and discriminant variable distributions are determined from interpolations between existing hA signals, obtaining distributions of $\chi^2(m_h, m_Z)$, where m_Z is the Z boson mass and m_h is ranging from 4 to 40 GeV/c^2.

A few hZ samples have been simulated (at m_h = 4, 20 and 40 GeV/c^2) to verify the validity of this procedure. Despite the different Higgs boson angular distributions and the Z boson width, the efficiencies and $\chi^2(m_h, m_Z)$ distributions proved accurate within the systematic errors estimated in the hA three-jet channel.

5.1.2 High mass search ($m_h > 40$ GeV/c^2)

The selection used to analyze the four-jet channel in the $e^+e^- \to ZZ$ cross-section measurement [19] is adapted to test the hypothesis of Higgs boson production. After the selection of high multiplicity events with at least four DURHAM jets, the only remaining backgrounds are from ZZ and WW four-quark final states, and four jet events arising from $q\bar{q}$ production with hard final state gluon radiation. Event shape variables and jet kinematics are used to further enhance the signal.

A constrained fit is performed on the reconstructed jets, requiring energy and momentum conservation between the

Table 4. hZ search, final state with jets. Numerical comparison between background simulation, data, and a few example signals, after an illustrative cut on P_{Higgs} that maximises the product of signal efficiency and purity. All data from 189 to 209 GeV are included. The signal normalization assumes $C^2_{hZ} = 1$. The statistical uncertainty on the signal efficiency and on the background is less than 1%

m_h (GeV/c^2)	SM (no hZ)	observed	ϵ_{hZ}(%)	hZ (h $\to$ q$\bar{q}$)
40	635.0	659	31.3	154.6
50	522.8	532	30.1	132.3
60	1784.1	1824	51.9	197.1
70	5457.3	5476	78.6	249.3
80	1681.7	1764	54.2	136.0
90	957.4	970	54.6	96.2
100	368.5	372	47.0	41.1
110	87.6	75	33.9	9.4

initial and final state. The fitted jet momenta are then used to reconstruct the dijet masses for all possible jet pairings. The uncertainties on the fitted momenta and their correlation matrix are taken into account in that procedure. The dijet masses and their uncertainties are used to compute the probability that each event is compatible with WW, ZZ, q$\bar{q}$, or hZ production (in this case, the event probability depends on the signal mass hypothesis), as in [19].

Finally, for each jet, the probability that it originates from a b quark is computed, using the methods described in [21]. Adding this information in the characterization of Z boson dijets allows better sensitivity to the fraction of the signal where the Z boson decays into b quarks. This information is not used on the Higgs boson side, thus preserving flavour-independence.

The method employed to combine the various mass, event shape and b-tagging probabilities using likelihood ratio products is described in [19]. The resulting discriminant variable is called P_{Higgs}.

Table 4 gives a numerical comparison between data and simulation, for a few Higgs boson masses. Examples of ln(P_{Higgs}) distributions are shown in Fig. 4. At each Higgs boson mass hypothesis, the P_{Higgs} distributions in data, background and signal are used for the statistical interpretation of the results (see Sect. 2). For every mass hypothesis, the signal distribution is obtained from an interpolation between the two closest simulated signal samples.

The systematic uncertainties are dominated by the uncertainty on the four-jet rate in q$\bar{q}$ events [22], conservatively taken to be 10% over the full Higgs boson mass range. Other contributions, evaluated in detail in [19], are small and can be neglected.

5.2 Final states with jets and missing energy

The event topology in the missing energy channel changes significantly as a function of the Higgs boson mass. For low enough Higgs boson masses a mono-jet final state is expected, while at high mass the jets are well separated, resulting in a two jet final state. For both mass domains (with

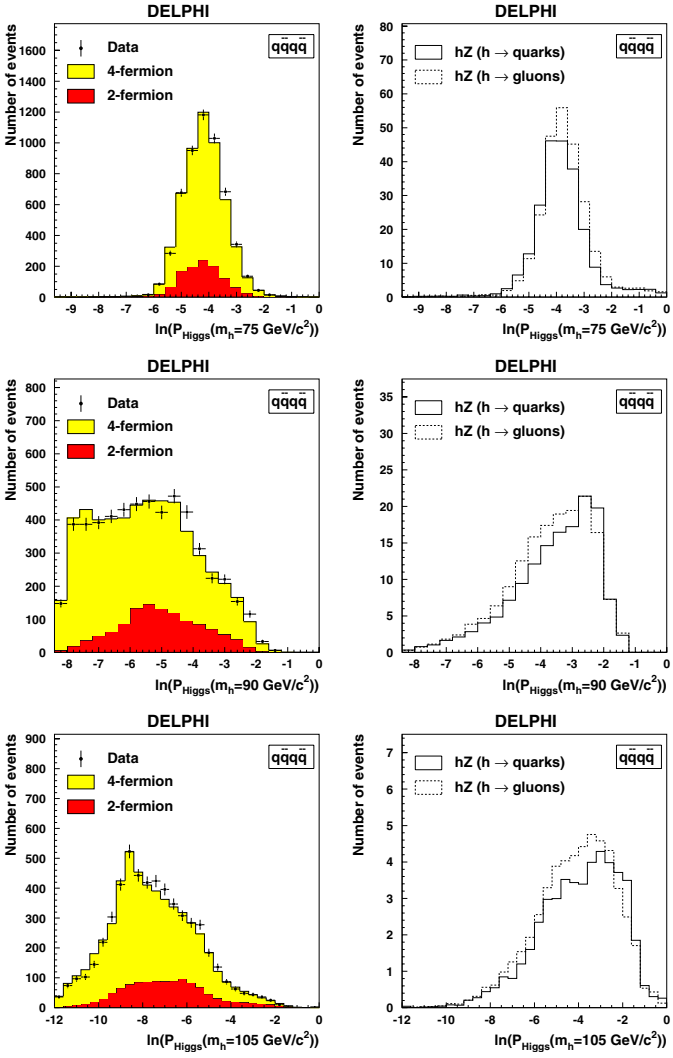

Fig. 4. hZ search, final state with jets. Comparison between data and simulation for the distributions of ln(P_{Higgs}). Higgs boson mass hypotheses of 75, 90 and 105 GeV/c^2 are shown from top to bottom. All data from 189 to 209 GeV are included. The signal normalization assumes $C^2_{hZ} = 1$

a transition set at m_h =40 GeV/c^2), dedicated analyses are described below.

5.2.1 Low mass search ($m_h < 40$ GeV/c^2)

The analysis used to measure the $Z\gamma^* \to \nu\bar{\nu}q\bar{q}$ cross-sections [20] is adopted without major modifications to test the hypothesis of low mass Higgs boson production in the missing energy channel. After a preselection reducing the $\gamma\gamma$, Bhabha and $Z\gamma$ backgrounds, three selections are designed, focusing on different expected topologies as a function of the mass of the Higgs boson.

The first selection is optimized to probe very low Higgs boson masses, using an explicit cut on the visible mass of the event, which is required to be below 6 GeV/c^2. The second selection exploits the large energy imbalance of h$\nu\bar{\nu}$ final states: events are split into two hemispheres according to the plane perpendicular to the direction of the thrust axis,

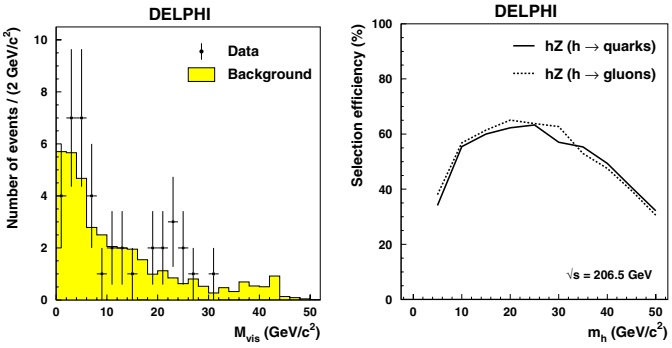

Fig. 5. hZ search, final state with jets and missing energy, low mass search. Left: comparison between data and simulation for the hadronic invariant mass distribution, after the monojet $\nu\bar{\nu}q\bar{q}$ event selection. All data from 189 to 209 GeV are included. Right: selection efficiency as a function of the Higgs boson mass, at $\sqrt{s} = 206.5\,\mathrm{GeV}$

and are required to have one of the hemispheres containing at least 99% of the total visible energy in the event. The third selection, which is less efficient at very low masses because of an explicit cut on the charged particle multiplicity, is mainly based on a topological requirement: events are forced into a two jet configuration and an upper cut on the opening angle of the two jets is set at 78 degrees. All three selections use the information from the veto counters, by rejecting events with hits in veto counters far away from energy depositions in calorimeters or reconstructed tracks. The three analyses are combined on an event-by-event basis, by selecting events that pass at least one cut.

After all selections, the most important remaining background processes are $Z\gamma^*$ and $We\nu$. Higgs boson signal efficiencies reach up to 65%, and drop to 40% for masses below $5\,\mathrm{GeV/c^2}$ and above $40\,\mathrm{GeV/c^2}$. The efficiencies are found to be independent, within their statistical uncertainties, of the quark or gluon nature of the Higgs boson decay. The reconstructed visible mass distribution is used as discriminant variable for the statistical evaluation of the compatibility of the data with the expectation for different Higgs boson mass hypotheses (see Sect. 2). For every mass hypothesis, the signal distribution is obtained from an interpolation between the two closest simulated signal samples. Higgs boson decays to gluons are assumed, given the worse mass resolution expected in this case. The reconstructed mass spectra and Higgs boson signal efficiencies are illustrated in Fig. 5.

The systematic uncertainty on the predicted background rate is 9%, obtained by varying each cut by an amount equal to the difference of the corresponding variable's average values in data and in simulation, at the preselection level. The uncertainty also includes a 5% contribution from the statistical uncertainty on the simulated background sample [20]). The uncertainty on the signal selection efficiency is 5%.

5.2.2 High mass search ($m_\mathrm{h} > 40\,\mathrm{GeV/c^2}$)

The selection described below closely follows the search for invisibly decaying Higgs bosons produced together with Z bosons decaying into hadrons [23]. Backgrounds originating from $q\bar{q}(\gamma)$ and $\gamma\gamma$ processes are rejected by applying the same selections as in [23]. Events with more than two identified leptons are then rejected. After this step, all events are clustered into both two-jet and three-jet configurations, using the DURHAM clustering algorithm.

To obtain a good performance over the mass range $40 < m_\mathrm{h} < 115\,\mathrm{GeV/c^2}$, three mass windows are defined ($40 \le m_\mathrm{h} < 70\,\mathrm{GeV/c^2}$, $70 \le m_\mathrm{h} < 90\,\mathrm{GeV/c^2}$, and $90 \le m_\mathrm{h} < 115\,\mathrm{GeV/c^2}$, subsequently referred to as first, second, and third mass range, respectively), and each is treated with a dedicated analysis. The discrimination is obtained in each case using a two-step Iterative Discriminant Analysis (IDA) [24]. After the first iteration, a cut on the IDA output is made to remove part of the background while retaining 90% of the signal. The IDA is then trained again on the events passing this selection. At each step, the IDA is trained simultaneously on $s\bar{s}$, $c\bar{c}$ and $b\bar{b}$ flavours, resulting in a comparable performance for all flavours.

Twelve variables compose the IDA discriminant for the first mass range. These are the scalar and vector sums of the transverse momenta of all reconstructed particles, the total visible energy, the event thrust, the energy of the least energetic jet in the three-jet configuration, the difference between the Fox-Wolfram moments H2 and H4 [25], the energy of the most isolated particle, the complement of the two jets opening angle (acollinearity), the angle between the two planes formed by the jet axes and the beam axis (acoplanarity), the total missing mass, and the highest transverse momentum of a particle with respect to its jet in the two-jet configuration. The IDA was trained with signal samples ranging from m_h =40 to $67.5\,\mathrm{GeV/c^2}$.

The analysis in the second mass range uses the same twelve variables as in the low mass analysis, except for the energy of the least energetic jet in the three-jet configuration, which is replaced by the event b-tag probability as defined in [21]. The IDA was trained with signal samples ranging from m_h =70 to $87.5\,\mathrm{GeV/c^2}$.

In the third mass range, the IDA is composed of the same variables as above, but cuts removing the tails in the distributions of the input variables are applied prior to the training, as is done in [23]. For every centre-of-mass energy, the IDA was trained on signal samples ranging from m_h $=90\,\mathrm{GeV/c^2}$ to the kinematic limit.

Numerical comparisons between data and simulation are given in Table 5, after the cut on the first IDA output.

The measured jet momenta are rescaled so that the missing mass equals m_Z, and the hadronic mass is computed using the rescaled jets. For each signal hypothesis, a window around the nominal Higgs boson mass is defined as a final selection, to maximize the product of signal efficiency and purity.

The second step discriminant variable, called IDA2, is used in the statistical interpretation of the analyses. For every mass hypothesis, the signal distribution is obtained from an interpolation between the two closest simulated signal samples. The IDA2 distributions are shown in Fig. 6, for events inside the final mass window. This figure also shows that a better separation between background and signal is obtained for gluonic Higgs boson decays.

Table 5. hZ search, final state with jets and missing energy, high mass search. Numerical comparison between background simulation, data, and a few example signals, just before the second IDA iteration. All data from 189 to 209 GeV are included. The signal normalization assumes $C^2_{\mathrm{hZ}} = 1$. The statistical uncertainty on the signal efficiency and on the background is less than 1%

m_{h} (GeV/c^2)	SM(no hZ)	observed	$\epsilon_{\mathrm{hZ}}(\%)$	hZ ($\mathrm{h} \to \mathrm{q\bar{q}}$)
40	5.5	6	44.1	62.4
50	8.7	8	40.7	51.2
60	16.2	18	39.7	43.1
70	82.8	72	43.0	39.0
80	165.2	155	45.8	32.9
90	257.9	238	50.6	25.5
100	121.4	124	44.6	11.2
110	66.9	76	42.0	3.3

The estimation of the systematic uncertainties also follows what was done in the search for invisible Higgs boson decays [23]. The dominant contribution originates from the description of the event shape variables, which affects the estimation of the $\mathrm{q\bar{q}}(\gamma)$ background. Calibration data taken at centre-of-mass energies close to the Z pole are used to evaluate these systematics using the method described in [19, 23]. Compared to these, the uncertainties on the background level due to the choice of jet clustering algorithm and the b-tagging procedure are small and can be neglected.

The uncertainties on the background vary from year to year due to different detector operating conditions, and are between 5.7% and 12.6% for the first mass range, between 6.2% and 10.2% for the second mass range, and between 4.0% and 8.2% for the third mass range. The corresponding systematic uncertainty on the signal efficiency is between 1 and 3%, the largest uncertainty affecting the first mass range.

5.3 Final states with jets and isolated leptons

The $\mathrm{q\bar{q}e^+e^-}$ and $\mathrm{q\bar{q}}\mu^+\mu^-$ channels are analysed in the same way as in the $\mathrm{e^+e^-} \to \mathrm{ZZ}$ and $\mathrm{Z}\gamma^*$ cross-section measurements. This search selects events with two identified leptons of the same flavour (electrons or muons) and of opposite charge, and at least two jets reconstructed with the JADE algorithm [26] (with $y_{min} = 0.01$). Compared to [19, 20], cuts on the invariant mass of the leptonic and hadronic systems (used to enrich the ZZ and $\mathrm{Z}\gamma^*$ samples) are not applied here, and the particle identification criteria are slightly modified in order to maximize the Higgs boson signal to background ratio.

The reconstructed mass of the hadronic system is used as discriminant in the statistical interpretation of the analyses. For every mass hypothesis, the signal distribution is obtained from an interpolation between the two closest simulated signal samples, and a window is defined around the nominal Higgs boson mass to maximize the signal to background ratio.

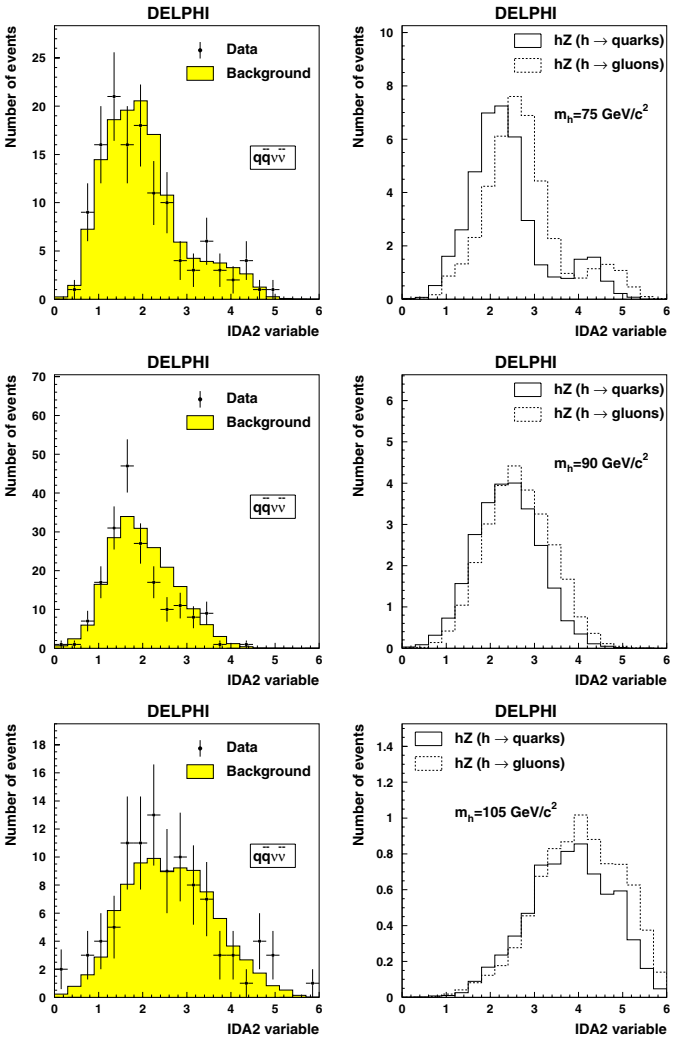

Fig. 6. hZ search, final state with jets and missing energy, high mass search. Comparison between data and simulation for the distributions of IDA2, after all selections. The distributions correspond to Higgs boson mass hypotheses of 75, 90 and 105 GeV/c^2 from top to bottom, respectively. All data from 189 to 209 GeV are included. The signal normalization assumes $C^2_{\mathrm{hZ}} = 1$

Distributions of the reconstructed hadronic mass are shown in Fig. 7. Tables 6 and 7 display the signal efficiencies, and a numerical comparison between data and simulation.

The main systematic uncertainties affecting the results are the uncertainty in the lepton identification and the signal selection efficiency. Combined with the statistical uncertainty from the finite size of the simulated sample, these result in a relative systematic uncertainty in selecting $\mathrm{q\bar{q}e^+e^-}$ and $\mathrm{q\bar{q}}\mu^+\mu^-$ events of 5%. The uncertainty on the small residual background rate is dominated by the MC statistics and amounts to 15%.

6 Results

The hypothesis of Higgs boson production is tested in this section, using the results from the analyses described above.

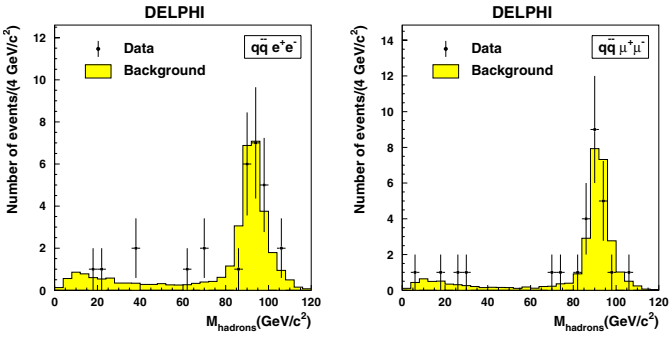

Fig. 7. hZ search, final state with jets and isolated leptons. Comparison between data and simulation for the reconstructed hadronic mass distribution, when the mass of the opposite lepton pair is within 15 GeV/c^2 of the Z mass. All data from 189 to 209 GeV are included

Table 6. hZ search, final state with jets and isolated electrons. Numerical comparison between background simulation, data, and a few example signals, after the mass cuts that maximize the separating power for each Higgs boson mass hypothesis. All data from 189 to 209 GeV are included. The signal normalization assumes $C^2_{\mathrm{hZ}} = 1$

m_{h} (GeV/c^2)	SM(no hZ)	observed	$\epsilon_{\mathrm{hZ}}(\%)$	hZ ($\mathrm{h} \to \mathrm{q\bar{q}}$)
40	1.6	3	59.8	14.2
50	1.1	2	61.8	12.9
60	1.5	3	63.3	11.4
70	2.3	4	63.4	9.5
80	17.6	18	66.1	7.9
90	23.3	18	69.5	5.8
100	16.3	11	68.2	2.8
110	1.9	3	64.2	0.8

Table 7. hZ search, final state with jets and isolated muons. Numerical comparison between data, background simulation, and a few example signals, after the mass cuts that maximize the separating power for each Higgs boson mass hypothesis. All data from 189 to 209 GeV are included. The signal normalization assumes $C^2_{\mathrm{hZ}} = 1$

m_{h} (GeV/c^2)	SM(no hZ)	observed	$\epsilon_{\mathrm{hZ}}(\%)$	hZ ($\mathrm{h} \to \mathrm{q\bar{q}}$)
40	1.5	3	77.1	18.1
50	2.3	4	77.5	16.1
60	2.0	3	78.5	14.1
70	3.3	3	76.8	11.5
80	20.0	16	78.0	9.3
90	25.6	20	80.6	6.7
100	17.8	18	81.1	3.3
110	3.1	2	76.8	0.9

The definition of the reference cross-sections, the statistical procedure, and the scope and limitations of the results are discussed in Sect. 2. The results are represented graphically in this paper, but explicit exclusion values can be obtained from the Collaboration on request.

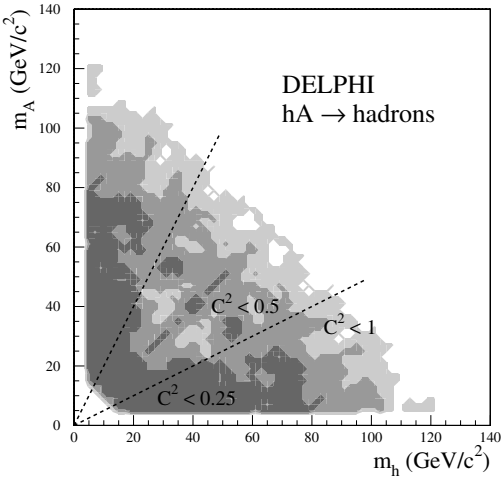

Fig. 8. Exclusion regions in the (m_{h},m_{A})-plane, for $0.5 \leq C^2_{\mathrm{hA}} \leq 1$, $0.25 \leq C^2_{\mathrm{hA}} \leq 0.5$, and $C^2_{\mathrm{hA}} \leq 0.25$ from light to dark grey. The dashed lines indicate the borders where the $\mathrm{h} \to \mathrm{AA}$ decay opens kinematically. The exclusions are given at the 95% CL

6.1 Excluded cross-sections for hA production

For each (m_{h},m_{A}) hypothesis, the $\chi^2(\mathrm{m_h}, \mathrm{m_A})$ distributions for background simulation, data and signal (see Fig. 2) are used as input to the statistical analysis.

The three analysis streams are combined as follows. The high-thrust stream is independent from the three-jet and four-jet streams, and is statistically combined with each of them in turn. The resulting combinations partly overlap, and cannot be added as independent channels. The ambiguity is solved at each mass point by choosing the combination that provides the strongest expected exclusion.

The mass domain is scanned from m_{h},$m_{\mathrm{A}} > 4$ GeV/c^2 to the kinematic limit, in mass steps of 1 GeV/c^2 in both directions. At each mass point, the confidence level in the background hypothesis is computed, and the value of C^2_{hA} that is excluded with a confidence level of exactly 95% is determined. No evidence for signal is observed. Figure 8 displays regions excluded in the (m_{h},m_{A})-plane, for a few fixed values of C^2_{hA}. For comparable Higgs boson masses and maximal production cross-section ($C^2_{\mathrm{hA}} = 1$), the combinations with $m_{\mathrm{h}} + m_{\mathrm{A}}$ below ~ 140 GeV/c^2 are excluded. When one of the Higgs bosons is very light, the mass of the other boson is constrained to be either below 4 GeV/c^2 (the hA search threshold), or above 108 GeV/c^2, still when $C^2_{\mathrm{hA}} = 1$. The three-jet and high-thrust analysis streams allow a significant portion of the mass plane to be excluded even when C^2_{hA} is as small as 0.25.

In most regions of the mass domain, the present search has high background and relatively low signal (see Fig. 2). The exclusions are thus very sensitive to fluctuations in the data, which explains the irregularities in the exclusion regions.

The above results are valid in the case of direct Higgs boson decays into hadrons. When the intermediate $\mathrm{h} \to \mathrm{AA}$ decay mode opens (the corresponding kinematic domain is delimited by the dashed lines in Fig. 8), the six-parton

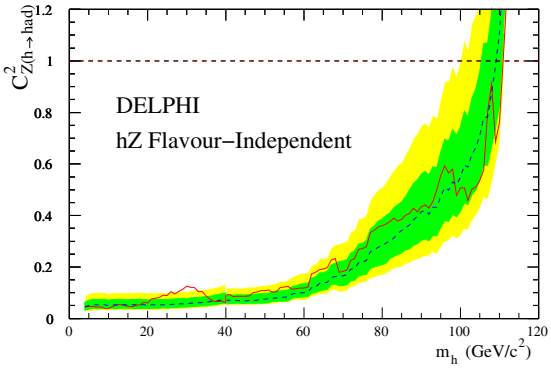

Fig. 9. Excluded values of C^2_{hZ} as a function of the Higgs boson mass, assuming direct hadronic Higgs boson decays. The solid curve is the observed exclusion, the median exclusion expected in the absence of signal is shown by the dashed curve, and the bands represent the 68% and 95% confidence intervals

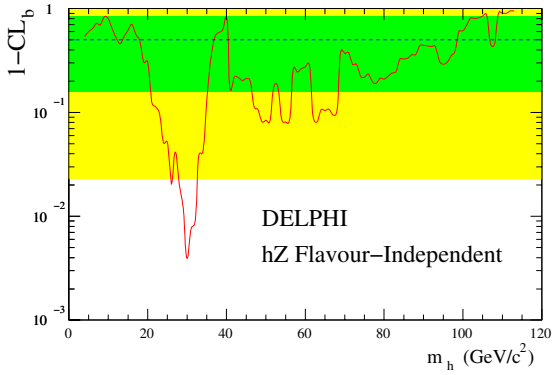

Fig. 10. Confidence level in the background hypothesis as a function of the Higgs boson mass. The solid curve is the observed confidence, the median expectation from background-only experiments is shown by the dashed line, and the bands represent the 68% and 95% confidence intervals

final state may become dominant. The sensitivity of the present analyses to this topology has not been evaluated.

As stated in Sect. 2, the hA exclusions are valid independently of the parity properties of h and A, and in particular may be interpreted in models with additional Higgs doublets or singlets, or in the context of a CP-violating Higgs sector.

6.2 Excluded cross-sections for hZ production

For each m_h hypothesis, the discriminant variables provided by the analysis channels described in Sect. 5 are used as input to the statistical analysis. For masses below 40 GeV/c^2, these are the $\chi^2(m_h, m_Z)$ distributions from the hadronic channel (like in Fig. 2), and the mass spectra from the low mass missing energy channel (see Fig. 5). Above 40 GeV/c^2, the hadronic channel provides distributions of $\ln(P_{Higgs}(m_h))$ (Fig. 4), the high mass missing energy search provides distributions of the second step IDA output, IDA2 (Fig. 6), and the channel with jets and leptons provides the hadronic mass distributions.

The Higgs boson mass domain is scanned from $m_h \geq 4$ GeV/c^2 to the kinematic limit. At each tested mass, the confidence level in the background hypothesis is computed, and the value of C^2_{hZ} excluded with a confidence level of exactly 95% is determined. The scan is done in steps of 1 GeV/c^2 over most of the range, and in steps of 100 MeV/c^2 when the excluded value of C^2_{hZ} approaches 1. Cross-section limits are computed for Higgs boson decays into either gluon or quark pairs, and the flavour-independent result at each mass is given by the weakest expected exclusion.

Figure 9 shows the excluded values C^2_{hZ} as a function of the Higgs bosons mass. Observed and expected limits agree well over a wide range of masses. The largest discrepancy occurs for a Higgs boson mass close to 30 GeV/c^2 where an excess of 2.65 σ is observed (the excess is around 2.5 σ when the result is averaged over the mass resolution at that particular Higgs boson mass hypothesis). The excess is shared by two channels: the missing energy channel contributes around 2 σ, and the low-mass fully hadronic channel contributes around 1.5 σ. The confidence level in the background hypothesis is shown as a function of m_h in Fig. 10. The confidence level in the background reaches a few 10^{-3} around m_h =30 GeV/c^2, but it should be remembered that given the large number of tested mass hypotheses, the probability that such an excess occurs at at least one mass is much larger.

Except for signal hypotheses around $m_h = 107$ GeV/c^2, there is a deficit of data in the hypothesis range $100 \leq m_h \leq 115$ GeV/c^2. The discrepancy is at the level of 1 to 1.5 σ, as can be seen in Fig. 10. The exclusions are thus stronger than expected in this region. Table 8 gives the mass limits for hadronic Higgs boson decays when $C^2_{hZ} = 1$, and for comparison the results achieved in the SM Higgs boson searches [27].

Table 8. The expected and observed 95% CL lower limits (in GeV/c^2) on the mass of a hadronically decaying Higgs boson, assuming its cross-section is identical to that in the SM. The results of the SM Higgs boson search are also given for comparison

	expected limit (GeV/c^2)	observed limit (GeV/c^2)
DELPHI ($h \to q\bar{q}$)	108.0	110.6
DELPHI ($h \to gg$)	109.2	111.0
DELPHI (SM decay)	113.3	114.1

7 Summary

Searches for hadronic Higgs boson decays have been performed, exploiting the LEP2 collision data recorded by DELPHI. No evidence of the presence of a signal was found in either the $e^+e^- \to hZ$ or the $e^+e^- \to hA$ process, in a mass range extending from 4 GeV/c^2 to the kinematic limit.

For the hZ process, a cross-section larger than 15% of the SM value (i.e $C^2_{hZ} > 0.15$) is excluded from m_h =4 to 60 GeV/c^2. Under the assumption of a production cross-section equal to that of the Standard Model, $m_h <$

$110.6\,\mathrm{GeV/c^2}$ is excluded at the 95% CL, while a limit of $108\,\mathrm{GeV/c^2}$ is expected on average from background-only experiments. The cross-section limit is weaker than expected around m_h =30 $\mathrm{GeV/c^2}$.

A large part of the mass domain available for the hA process was explored as well. In the case of full production strength and 100% branching fraction into hadrons (i.e. $C^2_\mathrm{hA} = 1$), the excluded region extends roughly up to m_h, m_A =108 $\mathrm{GeV/c^2}$ for the heavier Higgs boson, when the lighter one has a mass below $10\,\mathrm{GeV/c^2}$. When both masses are equal, m_h,$m_\mathrm{A} < 70\,\mathrm{GeV/c^2}$ is excluded. Even for reduced cross-sections, significant portions of the mass plane remain excluded.

Acknowledgements. We are greatly indebted to our technical collaborators, to the members of the CERN-SL Division for the excellent performance of the LEP collider, and to the funding agencies for their support in building and operating the DELPHI detector. We acknowledge in particular the support of Austrian Federal Ministry of Education, Science and Culture, GZ 616.364/2-III/2a/98, FNRS-FWO, Flanders Institute to encourage scientific and technological research in the industry (IWT), Belgium, FINEP, CNPq, CAPES, FUJB and FAPERJ, Brazil, Czech Ministry of Industry and Trade, GA CR 202/99/1362, Commission of the European Communities (DG XII), Direction des Sciences de la Matière, CEA, France, Bundesministerium für Bildung, Wissenschaft, Forschung und Technologie, Germany, General Secretariat for Research and Technology, Greece, National Science Foundation (NWO) and Foundation for Research on Matter (FOM), The Netherlands, Norwegian Research Council, State Committee for Scientific Research, Poland, SPUB-M/CERN/PO3/DZ296/2000, SPUB-M/CERN/PO3/DZ297/2000, 2P03B 104 19 and 2P03B 69 23(2002–2004) FCT – Fundação para a Ciência e Tecnologia, Portugal, Vedecka grantova agentura MS SR, Slovakia, Nr. 95/5195/134, Ministry of Science and Technology of the Republic of Slovenia, CICYT, Spain, AEN99-0950 and AEN99-0761, The Swedish Research Council, Particle Physics and Astronomy Research Council, UK, Department of Energy, USA, DE-FG02-01ER41155. EEC RTN contract HPRN-CT-00292-2002.

References

1. W. Loinaz, J. D. Wells, Phys. Lett. B **445**, 178 (1998); M. Carena, S. Mrenna, C. E. M. Wagner, Phys. Rev. D **60**, 075010 (1999); M. Carena, S. Heinemeyer, C. E. M. Wagner, G. Weiglein, hep-ph/9912223; M. Carena, J. Ellis, A. Pilaftsis, C. E. M. Wagner, Nucl. Phys. B **586**, 92 (2000)
2. J. F. Gunion, H. E Haber, G. L. Kane, S. Dawson, The Higgs Hunter's Guide, Addison-Wesley Publishing Company, 1990
3. X. Calmet, H. Fritzsch, Phys. Lett. B **496**, 190 (2000)
4. ALEPH Collaboration, A. Heister et al., Phys. Lett. B **544**, 25 (2002)
5. L3 Collaboration, P. Achard et al., Phys. Lett. B **583**, 14 (2004)
6. OPAL Collaboration, G. Abbiendi et al., Phys. Lett. B **597**, 11 (2004); Eur. Phys. J. C **40**, 317 (2005)
7. A. L. Read, in CERN Report 2000-005, p. 81 (2000)
8. E. Gross, G. Wolf, B. Kniehl, Z. Phys. C **63**, 417 (1994); Erratum Z. Phys. C **66**, 321 (1995)
9. P. Janot, in CERN Report 1996-01, Vol. 2, p. 309
10. DELPHI Collaboration, P. Aarnio et al., Nucl. Instrum. Methods A **303**, 233 (1991); Nucl. Instrum. Methods A **378**, 57 (1996)
11. P. Chochula et al. (DELPHI Silicon Tracker Group), Nucl. Instrum. Methods A **412**, 304 (1998)
12. S. Jadach, B. F. L. Ward, Z. Was, Comput. Phys. Commun. **130**, 260 (2000)
13. E. Accomando, A. Ballestrero, Comput. Phys. Commun. **1999**, 270 (1997); E. Accomando, A. Ballestrero, E. Maina, Comput. Phys. Commun. **150**, 166 (2003)
14. A. Ballestrero et al., Comput. Phys. Commun. **152**, 175 (2003)
15. T. Sjöstrand et al., Comput. Phys. Commun. **135**, 238 (2001)
16. F. A. Berends, R. Pittau, R. Kleiss, Comput. Phys. Commun. **85**, 437 (1995)
17. P. Abreu et al., Nucl. Instrum. Methods A **427**, 487 (1999)
18. S. Catani et al., Phys. Lett. B **269**, 432 (1991); N. Brown, W. J. Stirling, Z. Phys. C **53**, 629 (1992)
19. DELPHI Collaboration, J. Abdallah et al., Eur. Phys. J. C **30**, 447 (2003)
20. DELPHI Collaboration, J. Abdallah et al., $Z\gamma^*$ production in $\mathrm{e^+e^-}$ interactions at $\sqrt{s}$ = 183–209 GeV (To be submitted to Eur. Phys. J. C)
21. DELPHI Collaboration, J. Abdallah et al., Eur. Phys. J. C **32**, 185 (2004)
22. A. Ballestrero et al., CERN Report 2000-009 (2000), p. 137
23. DELPHI Collaboration, J. Abdallah et al., Eur. Phys. J. C **32**, 475 (2004)
24. T. G. M. Malmgren, Comput. Phys. Commun. **106**, 230 (1997); T. G. M. Malmgren, K. E. Johansson, Nucl. Instrum. Methods A **403**, 481 (1998)
25. G. C. Fox, S. Wolfram, Nucl. Phys. B **149**, 413 (1979)
26. T. Sjöstrand, Comput. Phys. Commun. **28**, 229 (1983)
27. DELPHI Collaboration, J. Abdallah et al., Eur. Phys. J. C **32**, 145 (2004)